Clinical Oral Investigations (2023) 27:7881–7888
https://doi.org/10.1007/s00784-023-05380-w

RESEARCH

Convex triangular vs. cylindrical field of view: how does the shape of the FOV affect radiation dose?

Deivi Cascante-Sequeira[1] · Christiano Oliveira-Santos[2] · Danieli Moura Brasil[2] · Gustavo M. Santaella[2] · Christine Swanson[3] · Megan Blackburn[3] · William C. Scarfe[2] · Francisco Haiter-Neto[1]

Received: 4 August 2023 / Accepted: 10 November 2023 / Published online: 23 November 2023

Abstract

Objective To compare the dosimetry between convex triangular fields of view (FOV) and similar dimension cylindrical FOVs of two cone-beam computed tomography (CBCT) models.

Methods Optically stimulated luminescence dosimeters (OSLDs) were placed in fiducial anatomical locations in an anthropomorphic phantom representing an adult head male for dosimetry scans. Convex triangular FOVs (100 × 80 mm/maxilla-mandible; 100 × 50 mm mandible; 100 × 50 mm/maxilla) from Veraviewepocs 3D R100 (J. Morita, Kyoto, Japan) (R100) and Veraview® X800 (J. Morita, Kyoto, Japan) (X800) and cylindrical FOVs from R100 and X800 (80 × 80 mm/maxilla-mandible; 80 × 50 mm/mandible; 80 × 50 mm/maxilla) were obtained, resulting in 12 different scan protocols. Equivalent doses for each relevant organ/tissue and the effective dose for each protocol were calculated. Mean effective doses were compared by the two-way analysis of variance (ANOVA) with Tukey's post hoc test to evaluate the effect of the FOV and device ($\alpha = 0.05$).

Results The effective doses ranged between 69 and 324 μSv for the convex triangular FOVs and 76 and 332 μSv for the cylindrical FOVs. Convex triangular FOVs from the R100 device had effective doses 2.3 to 15.3% lower than their corresponding cylindrical FOVs with similar height ($p < 0.05$), and that difference ranged between 8.8 and 11.8% for the X800 device ($p < 0.05$).

Conclusion Convex triangular fields of view delivered slightly lower effective doses than the cylindrical fields of view of similar dimensions in the R100 and X800 CBCT devices.

Clinical relevance Understanding the influence of the image geometry formation in effective dose allows optimization to reduce patient dose.

Keywords Dosimetry · Radiation protection · Cone-beam CT

Introduction

A major concern using cone-beam computed tomography (CBCT) in dentistry is the potential increase of cancer risk due to ionizing radiation stochastic effects. As the risk of cancer induction has no threshold, the radiation dose that patients are exposed to is crucial, as any dose can increase the probability of cancer development [1–5]. Patient radiation dose reduction by optimization is one of the tenets of the ALADAIP (As Low As Diagnostically Acceptable being Indication-oriented and Patient-specific) principle [6]. In CBCT, the appropriate selection of field of view (FOV) to the region of interest and diagnostic task can substantially reduce patient radiation dose.

A wide variety of CBCT devices are currently available in Dentistry [7]. Technological improvements in hardware and software (flat panel detectors, iterative reconstruction, X-ray beam collimation, optimized filtering, tube current modulation, and low dose protocols) allow for maintaining image quality while decreasing patient dose [8, 9]. The Veraviewepocs 3D R100 (R100) and Veraview X800

✉ Deivi Cascante-Sequeira
dantikes@gmail.com

[1] Department of Oral Diagnosis, Piracicaba Dental School, University of Campinas, Piracicaba, Brazil

[2] Department of Diagnosis & Oral Health, University of Louisville School of Dentistry, Louisville, KY, USA

[3] Department of Radiation Oncology, University of Louisville School of Medicine, Louisville, KY, USA

(X800) CBCT devices (J. Morita MFG. Corp. Kyoto, Japan) feature a 180° rotation convex triangular *Reuleaux* triangle) field of view (FOV) in addition to the typical cylindrical FOV. This *Reuleaux* triangle shape is observed in the axial reconstruction of the FOV. The *Reuleaux* triangle is a non-circular, equilateral shape with curves that maintain a constant width developed by Franz Reuleaux in the 19th century [10]. According to the manufacturer, the convex triangular FOV, which covers more volume than the 80 mm cylindrical FOV, may decrease patient dose by up to 15% while adapting to the parabolic shape of the dental arches.

Pauwels et al. (2012) estimated the effective doses numerous CBCT devices using different exposure protocols and projection geometries and reported a substantial range in doses between different CBCT devices [11]. Rottke et al. (2018) suggested that the effective dose of the convex triangular FOV of the R100 device was lower than the cylindrical FOV, but only assessed the 80 mm height convex triangular and cylindrical FOVs [9]. Furthermore, previous in vitro studies showed an influence of the image geometry formation of the convex triangular FOVs in the image quality [12–14]. A newer model, the X800, also provides a convex triangular FOV and, as of yet, no comparable dosimetry for either device or for cylindrical FOVs of similar height have been reported.

Understanding the dosimetry of the different CBCT devices allows consideration of different protocols to reduce patient dose via optimization based on scientific evidence. The present study is aimed at assessing the dosimetry of the convex triangular FOVs and comparing them with the cylindrical FOVs of similar dimensions in the R100 and X800 (J. Morita, Kyoto, Japan) CBCT devices.

Materials and methods

The head and neck portion of an anthropomorphic Rando phantom (Alderson Research Laboratories, Stanford, CT) representing an average adult male, embedded in synthetic rubber for tissue simulation and horizontally sliced, was used for the dosimetry scans (Fig. 1a). Optically stimulated luminescence dosimeters (OLSDs) (NanoDots, Landauer, Glenwood, IL) were calibrated using a calibration set provided by the manufacturer for the acquisition parameters used in the study. For each CBCT protocol, 24 OSLDs ($10 \times 10 \times 2$ mm) (Fig. 2) were placed in different anatomical locations according to previous studies (Table 1), and 3 OSLDs were placed outside the room to measure background radiation [15–18]. The phantom was previously scanned to determine the location and slice level of the anatomical structure that each OSLD represented. Vertical slots were created with a high-speed handpiece to hold the OSLDs in their determined positions (Fig. 1b).

Dosimetry scans

CBCT scans were performed using the R100 and X800 CBCT devices, both using continuous exposition radiation. Acquisition parameters are shown in Table 2. The FOV position for each scan protocol was determined by two-direction scout to simulate clinical conditions. Three exposures were performed for each scan protocol to ensure enough radiation reached the OSLDs. After each protocol, the OSLDs were read in a microSTARii reader (Landauer, Glenwood, IL), which had been previously calibrated using a set of 80-kVp reference dosimeters provided by the manufacturer (a beam energy calibration factor was used to correct variations in dosimeter sensitivity across a

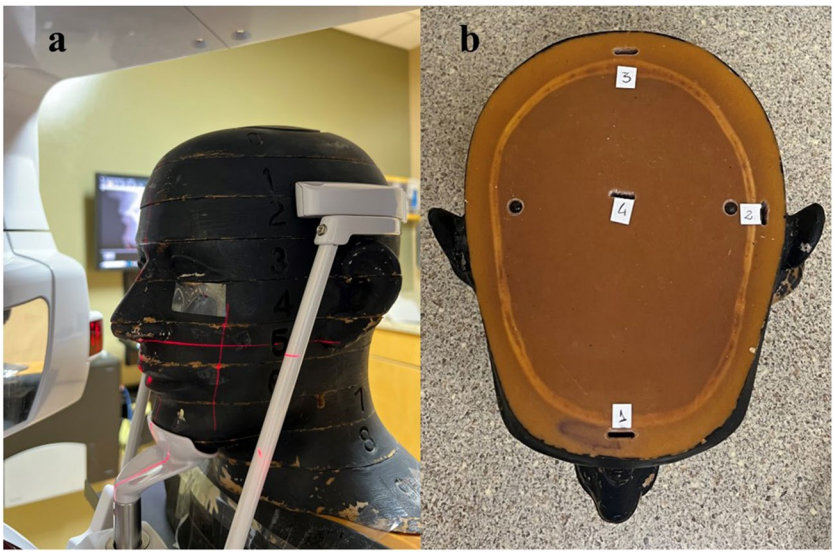

Fig. 1 Anthropomorphic phantom used in the different protocol scans. **a** Diagonal view of the phantom in the R100 device. **b** Numbered slots (arrows) at level 2 for holding the OSLDs within the phantom: 1. calvarium anterior; 2. calvarium left; 3. calvarium posterior; 4. midbrain)

Fig. 2 Close-up view and relative size of the Optically Stimulated Luminescent Dosimeters (OSLDs)

Table 1 Anatomical locations and slice level of the OSLDs

Dosimeter	Anatomical location	Slice level
1	Calvarium anterior	3
2	Calvarium left	3
3	Calvarium posterior	3
4	Midbrain	3
5	Pituitary	4
6	Right orbit	5
7	Left orbit	5
8	Right lens of eye	5
9	Left lens of eye	5
10	Right cheek	6
11	Right parotid	7
12	Left parotid	7
13	Right ramus	7
14	Left ramus	7
15	Center cervical spine	7
16	Left back of neck	8
17	Right mandible body	8
18	Left mandible body	8
19	Right submandibular gland	8
20	Left submandibular gland	8
21	Sublingual gland	8
22	Midline thyroid	9
23	Thyroid surface—left	9
24	Esophagus	9

range of beam energies). The measured background radiation was subtracted from the measured radiation of the experimental dosimeters. Each reading was divided by three to determine the absorbed dose of each OSLD per exposure. Before re-irradiation of the OSLDs, they were placed on a 150W 15,000 Lumen LED light for 30 minutes. This process of optical bleaching clears the stored signal in the device allowing for new measurements to be made. The OSLDS were then inserted into the same corresponding slots in the phantom slices for all the subsequent scans to reduce angular dependence [19]. Twelve protocols among two CBCT devices were scanned for dose calculations (Table 3).

Statistical analysis

Mean equivalent and effective doses and standard deviation values were calculated based on the OLSD absorbed dose readings and according to previous studies [16–18]. The equivalent doses for each of the following organs or tissues were calculated and multiplied by their estimated fraction irradiated in the exam: bone marrow (16.5%), esophagus (10%), thyroid (100%), bone surface (16.5%), brain (100%), salivary glands (100%), skin (5%), and remainder (oral mucosa, and extrathoracic tissue—100%, lymphatic nodes, and muscle—5%). Other tissues that comprise the remainder (i.e., adernals, gall bladder, heart, kidneys, pancreas, prostate, small intestine, spleen, and thymus) were considered to yield no radiation for these scans. The tissue weighting factors recommended by the International Commission on Radiological Protection Publication 103 were applied to calculate the effective doses for each protocol [1]. The mean effective doses were compared by the two-way analysis of variance (ANOVA) with the Tukey post hoc test to evaluate the effect of the FOV and device. All analyses were performed using IBM SPSS Statistics software v. 24.0 (IBM Corp., Armonk, NY),

Table 2 Technical parameters according to CBCT device and FOV shape and size

CBCT device	FOV shape	FOV size (mm)	Basis images	Voxel size (mm)
R100	**Convex triangular** ▲	100 Ø* × 50 h	401	0.125
		100 Ø* × 80 h	501	0.160
	Cylindrical ●	80 Ø × 50 h	401	0.125
		80 Ø × 80 h	641	0.125
X800	**Convex triangular** ▲	100 Ø* × 50 h	401	0.125
		100 Ø* × 80 h	641	0.125
	Cylindrical ●	80 Ø × 5 0 h	401	0.125
		80 Ø × 80 h	641	0.125

Fully standardized acquisition parameters: 90 kV, 8 mA, 180° rotation angle, ~9.4 s of acquisition time, and 0.2 mm copper filter. *Ø*, diameter; *Ø**, equivalent-diameter; *h*, height

Table 3 Scan protocols according to CBCT device and FOV shape, size, and region

CBCT device	FOV shape	FOV size (mm)	Region
R100	**Convex triangular** ▲	100 Ø* × 50 h	1. Mandible
			2. Maxilla
		100 Ø* × 80 h	3. Mandible-maxilla
	Cylindrical ●	80 Ø × 50 h	4. Mandible
			5. Maxilla
		80 Ø × 80 h	6. Mandible-maxilla
X800	**Convex triangular** ▲	100 Ø* × 50 h	7. Mandible
			8. Maxilla
		100 Ø* × 80 h	9. Mandible-Maxilla
	Cylindrical ●	80 Ø × 5 0 h	10. Mandible
			11. Maxilla
		80 Ø × 80 h	12. Mandible-maxilla

Ø, diameter; *Ø**, equivalent-diameter; *h*, height

adopting a significance level of 5%; a p value lower than 0.05 was considered significant. The null hypothesis was that the FOV, and device would not influence the effective dose.

Results

Table 4 shows the equivalent doses to each organ or tissue and mean effective dose and standard deviation for the different FOVs in the CBCT devices assessed. The effective doses ranged between 69 and 324 µSv for the convex triangular FOVs and between 76 and 332 µSv for the cylindrical FOVs. When comparing the effective dose between the convex triangular FOVs and the cylindrical FOVs of similar height (intra-device), the R100 device showed a reduction in the effective dose ranging from 2.3 to 15.3% ($p < 0.05$) and from 8.8 to 11.8% for the X800 device ($p < 0.05$). The lowest effective doses were found in the convex triangular FOVs restricted to the maxillary regions ($p < 0.05$). In contrast, the highest doses were observed in the cylindrical FOVs involving both maxillary and mandibular regions ($p < 0.05$). Furthermore, when comparing the R100 and X800 convex triangular FOVs with the same dimensions, doses were 48 to 57% higher in the R100 device ($p < 0.05$). The highest dose for the convex triangular FOVs corresponded to the R100 device ($p < 0.05$).

The average contribution of each organ to the effective dose is shown in Table 5. The highest equivalent doses to organ and tissues were measured in the salivary glands among all FOVs and devices, ranging from 1525 (X800) to 7760 µSv (R100 device). Furthermore, an average increase of 60% in the absorbed dose was observed in the thyroid among all FOVs of the R100 when compared with the X800. The highest contributions come from the remainder organs, followed by the salivary glands, thyroid gland, and bone marrow. The brain, bone surface, esophagus, and skin have minimal contributions.

Table 4 Equivalent doses to organs/tissues (μSv) and effective doses (μSv) according to FOV and CBCT device

Device	FOV	Equivalent doses to organs/tissues								Mean effective dose (SD)	
		Bone marrow	Esophagus	Thyroid	Bone surface	Brain	Salivary glands	Skin	Remainder*		95% confidence interval
R100	▲100 × 50 mandible	203	130	1279	654	186	5573	103	835	**246.15 (0.62) D**	244.57–247.77
	▲100 × 50 maxilla	224	42	455	722	451	3654	112	561	**163.73 (0.85) F**	161.68–165.36
	▲100 × 80	317	42	1591	1025	537	7072	207	1066	**324.95 (1.46) B**	321.21–327.59
	● 80 × 50 mandible	225	127	1425	726	203	6953	112	1013	**290.81 (1.89) C**	286.25–295.10
	● 80 × 50 maxilla	242	44	434	782	607	3884	139	626	**177.71 (0.99) E**	175.34–179.82
	● 80 × 80	314	130	1400	1016	553	7760	227	1144	**332.57 (1.28) A**	328.99–334.92
X800	▲100 × 50 mandible	120	50	575	386	97	2878	51	430	125.22 (0.49) D	124.00–126.42
	▲100 × 50 maxilla	95	15	163	308	273	1525	53	240	69.05 (0.22) F	68.50–69.58
	▲100 × 80	146	62	672	470	194	3183	90	481	144.04 (0.40) B	143.05–145.02
	● 80 × 50 mandible	128	57	636	414	109	3344	56	496	142.01 (0.52) C	140.70–143.31
	● 80 × 50 maxilla	99	17	190	321	267	1744	69	268	76.54 (0.17) E	76.15–76.90
	● 80 × 80	153	61	674	493	290	3654	103	539	157.33 (0.06) A	157.19–157.47

▲; convex triangular field of view; ●, cylindrical field of view. *SD*, standard deviation. *Lymphatic nodes, muscle, oral mucosa, extrathoracic tissue, adrenals, gall bladder, heart, kidneys, pancreas, prostate, small intestine, spleen, and thymus. Different capital letters indicate significant differences between FOVs within the same device. Bold values: differed from the X800 device within the same conditions ($p < 0.001$). According to two-way ANOVA with Tukey post hoc test (5% significance level) ($p < 0.05$)

Table 5 Average and relative contribution of each organ to the effective doses according to the CBCT device and FOV

Organ	CBCT device							
	R100				X800			
	▲		●		▲		●	
	Average (μSv)	%	Average (μSv)	%	Average (μSv)	%	Average (μSv)	%
Bone marrow	29.8	12.2	31.3	11.7	15.2	12.8	15.2	12.1
Esophagus	4.4	1.8	4.0	1.5	1.8	1.5	1.8	1.4
Thyroid	44.4	18.1	43.5	16.3	20.0	16.7	20.0	16.0
Bone surface	8.0	3.3	8.4	3.2	4.1	3.4	4.1	3.3
Brain	3.9	1.6	4.5	1.7	2.2	1.7	2.2	1.8
Salivary glands	54.3	22.2	62.0	23.2	29.1	22.4	29.1	23.2
Skin	1.4	0.6	1.6	0.6	0.8	0.6	0.8	0.6
Remainder								
Oral mucosa	53.7	21.9	60.7	22.8	28.4	22.2	28.4	22.7
Extrathoracic tissue	40.3	16.5	43.9	16.5	21.3	16.8	21.3	17.0
Muscle	2.3	0.9	3.4	1.3	1.1	1.0	1.2	1.0
Lymphatic nodes	2.3	0.9	3.4	1.3	1.1	1.0	1.2	1.0
Other *	0	0	0	0	0	0	0	0
Total	245	100	267	100	113	100	126	100

▲; convex triangular field of view; ●, cylindrical field of view. *Adrenals, gall bladder, heart, kidneys, pancreas, prostate, small intestine, spleen, thymus

Discussion

The present study evaluated organ/tissue equivalent doses and effective doses of convex triangular FOVs of the R100 and X800 CBCT devices and compared them with cylindrical FOVs of similar height and diameter of the same devices under standardized energetic parameters. It is essential to highlight that comparing devices and FOVs helps to understand the effective dose to which patients are exposed. This can assist oral and maxillofacial radiologists and dental practitioners in selecting the most appropriate FOV for a specific diagnostic need.

The convex triangular FOVs showed discreetly lower effective doses than the cylindrical FOVs of the same devices. A previous study suggested that the convex triangular FOV decreases the effective dose by modifying the characteristic isocentric trajectory observed in cylindrical FOVs and its consequent momentaneously augmentation of the radiation source to object distance, which diminishes the intensity of the X-ray beam [9]. Our study corroborates that hypothesis by assessing convex triangular FOVs of different heights on two CBCT devices and contrasting them with corresponding cylindrical FOVs of similar size. In this sense, the discreet dose reduction could be important when assessing larger extensions of the maxillomandibular complex since the convex triangular FOVs (100 × 50 mm and 100 × 80 mm) of the R100 and X800 CBCT devices cover a larger region than the cylindrical FOVs (80 × 50 mm and 80 × 80 mm) of the same devices.

A tendency in the effective dose results was observed among all FOVs and devices: the bimaxillary FOVs showed a greater effective dose, followed by the mandibular FOVs, while the maxillary FOVs showed the lowest effective dose. This tendency reflects the importance of the absorbed dose of the salivary glands into calculation of the effective dose, even when the remainder tissues are weighted twelve times higher [11]. Furthermore, this reinforces the impact of the location of the FOV in the calculation of effective dose [16]. The effective dose increases when the FOV height involves a considerable portion of the salivary glands.

Some device differences must be pointed out to understand the differences in the effective doses between the similar dimension FOVs of the devices assessed. First, the R100 and X800 devices are hybrid, i.e., they can be used to acquire panoramic and CBCT images. In both R100 and X800 panoramic image acquisition, the x-ray source is negatively angulated so that the projection beam can pass through the object in an inferior-superior direction. However, for the X800, the radiation source adjusts to become perpendicular to the object and detector, whereas in the R100, it remains negatively angled. Thus, the X-ray beam in the R100 device passes through more radiosensitive organs (thyroid, salivary glands, esophagus' soft tissue, and skin) than in the X800, which increases the final effective dose to the patient. In addition, the source-to-detector distance and consequently

the source-to-patient distance are different between devices. The X800 device presents longer distances (source-to-detector 60 cm and source-to-patient 40 cm) than the R100 device (source-to-detector 51.85 cm and source-to-patient 34.06 cm). In this sense, according to the inverse square law, the shorter the source-to-patient, the higher the intensity of the X-ray beam, and, consequently, higher the effective dose. Furthermore, when the source-to-detector distance is smaller, the beam needs to be more divergent to acquire the same field of view size as when the distance is larger. This increased divergence results in more exposure of the irradiated area, which leads to a higher effective dose due to direct and scattered radiation of radiosensitive organs. These differences explain the higher dose (up to 57%) in the convex triangular FOVs for the R100 device than in the X800 device. However, an earlier study revealed that when subjected to standardized energetic parameters (90 kV and 5 mA), the R100 device demonstrated a greater tendency towards shape distortion in high-density materials than the X800 device [13]. This observation suggests that reducing the tube current in the R100 device to compensate for the shorter source-to-detector distance may decrease image quality.

During the imaging process, both devices emitted continuous radiation, which could significantly impact the final effective dose. However, to avoid bias and prevent doubling the dose in the cylindrical FOVs, all FOVs were set to a 180° rotation angle. It is worth noting that the 100 × 80 mm convex triangular FOV of device R100 had fewer basis images than the FOV of similar dimensions for device X800, which also resulted in lower spatial resolution (according to raw data). The authors hypothesize that the acquisition velocity in the 100 × 80 mm convex triangular FOV of device R100 was faster than that of device X800. However, the effective dose in the 100 × 80 mm convex triangular FOV of device R100 was higher than that of device X800. This finding highlights the impact of the angulation of the X-ray beam on the final effective dose.

Concerning the contribution of organs to the effective dose, we found that in addition to the remainder tissues, the salivary glands, and thyroid glands, the bone marrow also significantly contributes to the effective dose, which agrees with a previous study assessing different CBCT devices [11]. However, we found a greater contribution of the esophagus to the effective dose. This could be explained because the most recent ICRP weighted tissue factors ponder these tissues with a higher impact in the final effective dose [1].

According to the manufacturer, the actual value of the convex triangular field of view is to cover more volume than the 80 mm cylindrical FOV while reducing the radiation dose. This is particularly useful for analyzing third molar regions that cannot be covered by the 80 mm cylindrical FOV. As the larger FOV in the R100 device is the convex triangular FOV, this is a reasonable option for covering both third molar regions simultaneously, above all, when it is necessary to compare both sides. On the other hand, the X800 device presents a 150 mm diameter FOV, but its resolution is lower than the convex triangular FOV. Even when our objective was not assessing image quality, it is crucial to consider this topic when discussing radiation dose. Thus, previous in vitro studies showed that the image quality of the convex triangular FOVs is lower than the cylindrical FOVs [12–14]. In this sense, the magnitude of artifacts in the convex triangular of the X800 device was greater than in the cylindrical FOVs [12]. Furthermore, the volumetric alteration artifact was influenced by the convex triangular FOV in both CBCT devices R100 and X800, with different manifestations among the materials assessed [14]. Finally, the shape distortion was even greater in the convex triangular FOVs than in the cylindrical FOVs of both R100 and X800 CBCT devices [13]. For this reason, it is essential to emphasize that even when the convex triangular FOVs assessed in the present study showed lower effective doses than the cylindrical FOVs, this reduction may be irrelevant. Therefore, there is still the need to evaluate in clinical conditions the relationship radiation dose-image quality for an appropriate dose optimization and the ALADAIP principle [6]. Thus, assessing diagnostic tasks related to the third molar regions is crucial to determine the real benefit of the convex triangular FOVs.

The present study used OSLDs for the dosimetry measurements, which present advantages over thermoluminescent dosimeters (TLDs). OSLDs can be re-used after each cycle of scans and dose readings, which could be beneficial for data recovery [20, 21]. One potential disadvantage of OSLDs is their angular dependence due to their geometric shape. However, a previous study has shown that the angular dependence of the OSLDs for radiation dose measurements is subtle [19]. In the current study, the OSLDs were placed in the same position for all scan protocols to ensure consistency.

Conclusion

The convex triangular fields of view delivered slightly lower effective doses than the cylindrical fields of view of similar dimensions in the R100 and X800 CBCT devices.

Acknowledgements The first author is grateful to the University of Costa Rica for funding his postgraduate studies.

Author contribution All authors contributed to the study conception and design and assume full responsibility for its content. Data acquisition was performed by D.C.-S. and C.d.O.-S.; analysis and interpretation of data for the work were done by D.C.-S., C.d.O.-S., D.M.B., G.M.S., C.S., M.B., W.S., and F.H.-N. The first draft of the manuscript was written by D.C.-S., and all authors commented on previous versions of the manuscript. All authors read and approved the final manuscript to be published.

Funding The first author's postgraduate studies are funded by a scholarship given by the Universidad de Costa Rica. This study was financed in part by the Coordenação de Aperfeiçoamento de Pessoal de Nível Superior – Brasil (CAPES) – Finance Code 001.

Declarations

Ethics approval and consent to participate Not applicable.

Conflict of interest The authors declare no competing interests.

References

1. ICRP (2007) The 2007 recommendations of the International Commission on Radiological Protection. ICRP publication 103. Ann ICRP 37(2-4):1–332
2. ICRP (2015) Radiological protection in cone beam computed tomography (CBCT). ICRP Publication 129. Ann ICRP 44(1):9–127
3. Lurie A, Kantor M (2020) Contemporary radiation protection in dentistry: recommendations of National Council on Radiation Protection and Measurements Report No. 177 - PubMed. J Am Dent Assoc 151(10):716–719.e3
4. FDI World Dental Federation (2014) FDI policy statement on radiation safety in dentistry: adopted by the FDI General Assembly. Int Dent J 64(6):289–290
5. European Commission (2012) Radiation Protection 172. Cone beam CT for dental and maxillo-facial radiology. Evidence-based guidelines. [Internet]. Luxembourg City, Luxembourg: European Commission Directorate for Energy; http://www.sedentexct.eu/files/radiation_protection_172.pdf
6. Oenning AC, Jacobs R, Salmon B, DIMITRA Research Group (2021) ALADAIP, beyond ALARA and towards personalized optimization for paediatric cone beam CT. Int J Paediatr Dent 12. https://doi.org/10.1111/ipd.12797
7. Gaêta-Araujo H, Alzoubi T, Vasconcelos KF, Orhan K, Pauwels R, Casselman JW, Jacobs R (2020) Cone-beam computed tomography in dentomaxillofacial radiology: a two-decade overview. Dentomaxillofac Radiol 49(8):20200145. https://doi.org/10.1259/dmfr.20200145
8. Kiljunen T, Kaasalainen T, Suomalainen A, Kortesniemi M (2015) Dental cone beam CT: a review. Phys Med 31:844–860. https://doi.org/10.1016/j.ejmp.2015.09.004
9. Rottke D, Dreger J, Sawada K, Honda K, Schulze D (2018) Comparison of manual and dose reduction modes of a MORITA R100 CBCT. Dentomaxillofac Radiol 47:20180009
10. Griffiths D, Culpin D (1975) Pi-optimal polygons. Math Gaz 59:165–175 http://www.jstor.org/stable/3617699
11. Pauwels R, Beinsbergera J, Collaertb B, Theodorakouc C, Rogerse J et al (2012) Effective dose range for dental cone beam computed tomography scanners. Eur J Radiol 81:267–271. https://doi.org/10.1016/j.ejrad.2010.11.028
12. Cascante-Sequeira D, Coelho-Silva F, Rosado LPL, Freitas DQ, de-Azevedo-Vaz SL, Haiter-Neto F (2022) Comparison of the expression of the volumetric alteration artifact in cylindrical and triangular fields of view in two cone-beam computed tomography devices. Clin Oral Investig 26: 1025–1033.
13. Cascante-Sequeira D, Coelho-Silva F, Lopes Rosado LP, Lucca LV, Queiroz Freitas D, Lins de-Azevedo-Vaz S, et al. (2023) Does cone-beam CT convex triangular field of view influence the image shape distortion of high-density materials? Dentomaxillofac Radiol. https://doi.org/10.1259/dmfr.20230029
14. Cascante-Sequeira D, Fontenele RC, Martins LAC, Brasil DM, Oliveira ML, Freitas DQ et al (2023) Does the shape of the field-of-view influence the magnitude of artefacts from high-density materials in cone-beam computed tomography? Dentomaxillofac Radiol. https://doi.org/10.1259/dmfr.20230147
15. Ludlow JB, Walker C (2013) Assessment of phantom dosimetry and image quality of i-CAT FLX cone-beam computed tomography. Am J Orthod Dentofacial Orthop 144:802–817. https://doi.org/10.1016/j.ajodo.2013.07.013
16. Pauwels R, Zhang G, Theodorakou C, Walker A, Bosmans H et al (2014) Effective radiation dose and eye lens dose in dental cone beam CT: effect of field of view and angle of rotation. Br J Radiol 87:1042
17. Ludlow JB, Ivanovic M (2008) Comparative dosimetry of dental CBCT devices and 64-slice CT for oral and maxillofacial radiology. Oral Surg Oral Med Oral Pathol Oral Radiol Endod 106(1):106–114
18. Ludlow JB, Timothy R, Walker C, Hunter R, Benavides E, Samuelson DB et al (2015) Effective dose of dental CBCT—a meta analysis of published data and additional data for nine CBCT units. Dentomaxillofac Radiol 44:20140197
19. Okasaki T, Hayashi H, Takegami K, Okino H, Kimoto N et al (2015) Fundamental study of nanoDot OSL dosimeters for entrance skin dose measurement in diagnostic X-ray examinations. J Radiat Protect Res 41(3):229–236
20. Akselrod MS, BØtter-Jensen L, SWS MK (2007) Optically stimulated luminescence and its use in medical dosimetry. Radiat Meas 41:7899
21. Jursinic PA (2007) Characterization of optically stimulated luminescent dosimeters, OSLDs, for clinical dosimetric measurements. Med Phys 34(12):4594–4604